Construction of an Exact Pressure-Equilibrium Scheme for the Five-Equation Two-Phase Flow Model with Thermal Relaxation

Nguyen Ly*, Christopher DeGrendele**,
Francois Cadieux**, Michael Barad**, and Jared Duensing**
Corresponding author: nguyen.ly@nasa.gov
* Analytical Mechanics Associates, Moffett Field, CA, United States
** NASA Ames Research Center, Moffett Field, CA, United States

Abstract: Numerical simulation of compressible multiphase flows based on the four-equation (homogeneous relaxation) model is known to suffer from two fundamental difficulties with (a) wave propagation and (b) pressure equilibrium preservation. First, the mixture sound speed exhibits non-monotonic dependency with respect to the volume fraction, which leads to robustness issues in the resolution of shocks and acoustic wave propagation across two-phase regions. This difficulty can be mitigated by solving Allaire's five-equation model augmented with infinitely fast phasic temperature equilibrium, from which solutions of the four-equation model can be recovered. However, when temperature is non-uniform, this augmented five-equation formulation still fails to preserve pressure equilibrium across material interfaces. In this work, we propose a fully conservative numerical scheme that exactly preserves pressure equilibrium at the discrete level for the augmented five-equation model, for arbitrary initial distributions of temperature and volume fraction. Combined with the monotonic sound speed property of the five-equation formulation, the proposed pressure-equilibrium preserving scheme significantly improves robustness in the presence of strong multiphase interactions, including shock–interface interactions and advection of material interfaces.

Keywords: Numerical Algorithms, Multiphase, Pressure-equilibrium Preserving.

1. Introduction

In multiphase flow simulations, a common strategy is to adopt an Eulerian formulation and model the mixture of the multiple phases as a single effective fluid with averaged properties based on the local volume fractions of each phase. Within this framework, a hierarchy of models exists, ranging from the non-equilibrium seven-equation model of Baer and Nunziato [1], to the five-equation model of Allaire et al. [2], which assumes instantaneous mechanical equilibrium between the phases, and finally to the four-equation model, also known as the homogeneous relaxation model (HRM) [3], which further assumes thermal equilibrium.

Because mechanical and thermal equilibrium are physically relevant assumptions for many engineering multiphase flow scenarios, the four-equation model is often the preferred choice under such conditions [4]. However, when solving the four-equation model numerically using low-dissipation schemes designed to avoid excessive smearing of material interfaces, robustness issues may arise in resolving shocks and acoustic waves across multi-phase regions. These numerical difficulties can be traced to the non-monotonic dependency of the mixture sound speed on the volume fraction, a behavior analogous to that of Wood's sound-speed formulation [3].

To address the robustness issues associated with the direct numerical solution of the four-equation model, one approach is to recover its solution by augmenting Allaire's five-equation model with an infinitely fast temperature relaxation term in the volume-fraction equation [5]. It has been shown that the solution of this augmented five-equation formulation is equivalent to that of the four-equation model [5]. The augmented system can be efficiently solved using a split-step strategy, in which the hyperbolic five-equation model and the local temperature relaxation term are integrated separately in time. This approach exhibits superior robustness compared to direct solution of the four-equation system, owing to the monotonic dependency of the mixture sound speed with respect to volume fraction in the hyperbolic five-equation step.

Another advantage of this approach is that, when employing contact-preserving numerical schemes, the numerical solution of Allaire's five-equation model maintains pressure and velocity equilibrium across material interfaces [2]. This pressure-equilibrium property also extends to the post-relaxation solution of the augmented system, but only in the special case of a spatially uniform initial temperature field. Consequently, while the augmented five-equation approach offers an advantage over the direct numerical solution of the four-equation model, where the construction of fully conservative pressure-equilibrium-preserving schemes remains an active area of research, this advantage is realized only under the restrictive assumption of constant initial temperature. In practical compressible multiphase flows, however, temperature variations across material interfaces are ubiquitous.

Recent progress has been made in the construction of exact and approximate pressure-equilibrium-preserving (PEP) conservative schemes for the four-equation model [6, 7]. In particular, DeGrendele et al. [8] proposed a general framework for constructing exact PEP conservative schemes for arbitrary equations of state, based on solving the discrete PEP criterion as a correction to an underlying numerical scheme. Nevertheless, these approaches do not resolve the previously discussed issue of non-monotonic mixture sound speed across interfacial layers, which continues to challenge robustness in the four-equation model.

In this work, we extend recent developments in exact PEP scheme construction to Allaire's five-equation model coupled with thermal relaxation. Our goal is to enhance the robustness of the augmented five-equation model by ensuring exact pressure-equilibrium preservation during the advection of material interfaces, even in the presence of non-uniform temperature distributions.

2. Governing Equations

In this study, we develop the numerical scheme on a uniform Cartesian grid. The formulation is applicable to general engineering configurations using non-conformal block-structured mesh refinement and immersed boundary methods [5]. Without loss of generality, the analysis is presented for the one-dimensional system.

We consider a first-order-in-time split-step approach for the solution of the augmented Allaire's five-equation model. In this context, the non-stiff hyperbolic equation,

$$\begin{aligned}
\frac{\partial(\rho Y_k)}{\partial t} + \frac{\partial(\rho Y_k u)}{\partial x} &= 0, \\
\frac{\partial(\rho u)}{\partial t} + \frac{\partial(\rho u u + p)}{\partial x} &= 0, \\
\frac{\partial(\rho E)}{\partial t} + \frac{\partial\left[(\rho E + p)u\right]}{\partial x} &= 0, \\
\frac{\partial \phi}{\partial t} + u\frac{\partial \phi}{\partial x} &= 0,
\end{aligned}$$

is solved first from time t_n to t_{n+1}. Here, $\rho, p, E = e + u^2/2$ are the fluid density, pressure, and total specific energy, respectively. e is the fluid specific internal energy, and u is the flow velocity. Furthermore, Y_k denotes the mass fraction of phase k and ϕ denotes the mass fraction of the liquid phase (assumed to be $k = 1$).

The solution of the hyperbolic step is then followed by a thermal relaxation step where the volume fraction is readjusted such that temperatures of the two phases are in equilibrium,

$$\frac{\partial(\rho Y_k)}{\partial t} = 0, \quad \frac{\partial(\rho u)}{\partial t} = 0, \quad \frac{\partial(\rho E)}{\partial t} = 0, \quad \frac{\partial \phi}{\partial t} = H(T_1 - T_2), \tag{1}$$

where $H \to \infty$ is the infinitely-fast thermal relaxation rate. In practice, the steady-state solution of Eq. (1) is recasted into an algebraic equation to solve for ϕ under the constraint of temperature equilibrium between the phases $T_1 = T_2$ and constant energy and phasic densities.

One again, note that ϕ is the volume fraction of the first (liquid) phase, such that $\phi_1 = \phi$ and $\phi_2 = (1-\phi_1)$. Then, the thermodynamic equation of state of the multiphase mixture is expressed under the condition of mechanical equilibrium (single pressure),

$$\rho = \sum_{k=1}^{2} \phi_i \rho_i = \sum_{k=1}^{2} \rho Y_i, \quad \rho e = \sum_{k=1}^{2} \phi_k \rho_k e_k.$$

Furthermore, we use the stiffened-gas equation of state (EOS) for the thermodynamics of each individual phase,

$$\frac{p_k}{(\gamma_k - 1)} + \frac{\gamma_k p_k^\infty}{(\gamma_k - 1)} = \rho_k(e_k - q_k), \quad \text{and} \quad T_k = \frac{(p_k + p_k^\infty)}{\left[(\gamma_k - 1)\rho_k c_{v,k}\right]},$$

where $p_1 = p_2 = p$ and $\gamma, c_{v,k}, p_k^\infty$, and q_k are the constant heat-capacity ratio, constant-volume heat capacity, stiffened-gas parameter, and energy datum (used for latent-heat calculation) for each phase, respectively.

3. Derivation of pressure-equilibrium preserving scheme

Typical hybrid schemes [9] for the hyperbolic step combine a low-dissipation central flux with a robust upwind flux based on an approximate Riemann solver. In this approach, the upwind scheme provides stability in regions of strong shocks, while the central flux reduces dissipation in regions of contact-line advection. Because pressure-equilibrium preservation is most critical in contact-line regions, our analysis focuses on the pressure dynamics of the low-dissipation central flux scheme. Extension of this analysis to the upwind flux is reserved for future work.

For the central-flux scheme, we employ the split form of the Kinetic Energy Entropy Preserving (KEEP) scheme [10].

Consider a solution of the multispecies 1D Euler equation using the method of lines, where a spatial discretization is employed to convert the PDE system into an ODE system of the discretized flow variables in time

$$\begin{aligned}
\left.\frac{d(\rho Y_1)}{dt}\right|_m + \left.F_{\rho Y_1}\right|_m &= 0 \\
\left.\frac{d(\rho Y_2)}{dt}\right|_m + \left.F_{\rho Y_2}\right|_m &= 0 \\
\left.\frac{d(\rho u)}{dt}\right|_m + \left.F_{\rho u}\right|_m &= 0 \\
\left.\frac{\partial(\rho E)}{\partial t}\right|_m + \left.F_{\rho E}\right|_m &= 0 \\
\left.\frac{d\phi}{dt}\right|_m + \left.F_{\phi}\right|_m &= 0
\end{aligned}$$

where $\left.F_{\rho Y_1}\right|_m, \left.F_{\rho Y_2}\right|_m, \left.F_{\rho u}\right|_m, \left.F_{\rho E}\right|_m, \left.F_{\phi}\right|_m$ are the discretized convective flux operators and m is the spatial grid point index. Then, for the transport of mass, momentum, and energy, the standard split KEEP scheme can be expressed as

$$
\begin{aligned}
F_{\rho Y_1}\Big|_m &= \frac{C_1|_{m+\frac{1}{2}} - C_1|_{m-\frac{1}{2}}}{\Delta x} \\
F_{\rho Y_2}\Big|_m &= \frac{C_2|_{m+\frac{1}{2}} - C_2|_{m-\frac{1}{2}}}{\Delta x} \\
F_{\rho u}\Big|_m &= \frac{M|_{m+\frac{1}{2}} - M|_{m-\frac{1}{2}}}{\Delta x} + \frac{\Pi|_{m+\frac{1}{2}} - \Pi|_{m-\frac{1}{2}}}{\Delta x} \\
F_{\rho E}\Big|_m &= \frac{K|_{m+\frac{1}{2}} - K|_{m-\frac{1}{2}}}{\Delta x} + \frac{I|_{m+\frac{1}{2}} - I|_{m-\frac{1}{2}}}{\Delta x} + \frac{S|_{m+\frac{1}{2}} - S|_{m-\frac{1}{2}}}{\Delta x},
\end{aligned}
$$

where

$$C_1|_{m+\frac{1}{2}} = \rho Y_1|_{m+\frac{1}{2}} \frac{u|_m + u|_{m+1}}{2} \tag{2}$$

$$C_2|_{m+\frac{1}{2}} = \rho Y_2|_{m+\frac{1}{2}} \frac{u|_m + u|_{m+1}}{2} \tag{3}$$

$$M|_{m+\frac{1}{2}} = \rho|_{m+\frac{1}{2}} \frac{u|_m + u|_{m+1}}{2} \frac{u|_m + u|_{m+1}}{2} \tag{4}$$

$$\Pi|_{m+\frac{1}{2}} = \frac{p|_m + p|_{m+1}}{2} \tag{5}$$

$$K|_{m+\frac{1}{2}} = \rho|_{m+\frac{1}{2}} \frac{u|_m + u|_{m+1}}{2} \frac{u|_m\, u|_{m+1}}{2} \tag{6}$$

$$I|_{m+\frac{1}{2}} = \rho e|_{m+\frac{1}{2}} \frac{u|_m + u|_{m+1}}{2} \tag{7}$$

$$S|_{m+\frac{1}{2}} = \frac{u|_m\, p|_{m+1} + u|_{m+1}\, p|_m}{2} \tag{8}$$

Following the split KEEP form, the volume fraction transport equation is discretized as follows:

$$\left.\frac{\partial \phi}{\partial t}\right|_m + \frac{\phi|_{m+\frac{1}{2}}\, u|_{m+\frac{1}{2}} - \phi|_{m-\frac{1}{2}}\, u|_{m-\frac{1}{2}}}{\Delta x} - \phi|_m \frac{u|_{m+\frac{1}{2}} - u|_{m-\frac{1}{2}}}{\Delta x} = 0.$$

When the mid-point values for ρY_k, ρe, and α are defined as the algebraic mean of the left and right states, we refer to this approach as the traditional KEEP scheme. The goal of our present analysis is to compose alternative definitions for these mid-point values such that the pressure-equilibrium condition can be enforced.

In the method of lines, the conserved variables $\rho Y_1, \rho Y_2, \rho u, \rho E, \phi$ are directly updated in the hyperbolic substep using time-stepping of the semi-discrete ODEs. On the other hand, the derived variables p, T_1, T_2 are indirectly updated from the conserved variables via

$$(p, T_1, T_2) = \mathrm{EOS}(\rho e, \rho Y_1, \rho Y_2, \phi) = \mathrm{EOS}\left(\rho E - \frac{1}{2}\frac{(\rho u)^2}{\rho}, \rho Y_1, \rho Y_2, \phi\right)$$

For the overall augmented scheme to be pressure-equilibrium preserving, the sufficient condition is that after one update of the hyperbolic substep for the pressure-equilibrium initial condition at time step t_n, $u|_m^n = U_0$, $p|_m^n = p_0$, and $T_1|_m^n = T_2|_m^n$ for each grid index m, the following criteria are satisfied for each grid index

$$u|_m^{n+1} = U_0 \quad (9)$$

$$p|_m^{n+1} = p_0 \quad (10)$$

$$T_1|_m^{n+1} = T_2|_m^{n+1} ., \quad (11)$$

where U_0 and p_0 are the initial constant velocity and pressure fields, respectively. Note that the temperature equilibrium condition Eq. (11) is required so that the thermal relaxation step Eq. (1) does not reintroduce a pressure non-equilibrium by relaxing the species temperatures towards one another.

First, we analyze the velocity-equilibrium aspect of the scheme. Analyzing velocity equilibrium first ensures that no artificial momentum errors propagate into the pressure field, allowing a clean assessment of the pressure-equilibrium condition. Expanding the velocity in a Taylor series with respect to the conserved variables and then assuming a single-step (i.e. Euler) temporal scheme for the update of flow variables from time t_n to time t_{n+1} gives

$$\begin{aligned} u|_m^{n+1} - u|_m^n &= \left(\frac{\partial u}{\partial \rho u}\right)_\rho\Bigg|_m^n (\rho u|_m^{n+1} - \rho u|_m^n) + \left(\frac{\partial u}{\partial \rho}\right)_{\rho u}\Bigg|_m^n (\rho|_m^{n+1} - \rho|_m^n) + \text{H.O.} \\ &= -\frac{1}{\rho|_m^n} F_{\rho u}\big|_m^n \Delta t + \frac{U_0}{\rho|_m^n}(F_{\rho Y_1}\big|_m^n + F_{\rho Y_2}\big|_m^n)\Delta t + \text{H.O.} \end{aligned}$$

Here, we only collect the leading order terms in the time stepping, leading to a first-order global convergence of the velocity equilibrium property. Substituting the KEEP scheme into the (implicit) velocity update rule, under the assumption of constant velocity and pressure at time step t_n, gives

$$u|_m^{n+1} - u|_m^n = \frac{U_0^2}{\rho|_m}\left[-\left(\rho|_{m+\frac{1}{2}}^n - \rho|_{m-\frac{1}{2}}^n\right) + \left(\rho Y_1|_{m+\frac{1}{2}}^n - \rho Y_1|_{m-\frac{1}{2}}^n\right) + \left(\rho Y_2|_{m+\frac{1}{2}}^n - \rho Y_2|_{m-\frac{1}{2}}^n\right)\right]\frac{\Delta t}{\Delta x} + \text{H.O.}$$

From here, we see that with the choice of mid-point density

$$\rho|_{m+\frac{1}{2}} \equiv \rho Y_1|_{m+\frac{1}{2}} + \rho Y_2|_{m+\frac{1}{2}} ,$$

the velocity equilibrium criterion Eq. (9) is satisfied with first order global convergence in time *for all grid spacing*. In this manner, we refer to the present scheme as being *spatially exact* in preserving velocity equilibrium.

For the pressure and temperature criteria Eqs. (10) and (11), since the update will consider the internal energy through the EOS, we first look at the implicit update rule for $\rho e = \rho E - \frac{1}{2}(\rho u)^2/\rho$. Expanding ρe in a Taylor series with respect to the conserved variables and then assuming a single-step (i.e. Euler) temporal scheme for the update of flow variables from time t_n to time t_{n+1} gives

$$\begin{aligned} \rho e|_m^{n+1} - \rho e|_m^n = &\left(\frac{\partial \rho e}{\partial \rho E}\right)_{\rho u,\rho}\Bigg|_m^n (\rho E|_m^{n+1} - \rho E|_m^n) + \left(\frac{\partial \rho e}{\partial (\rho u)}\right)_{\rho E,\rho}\Bigg|_m^n (\rho u|_m^{n+1} - \rho u|_m^n) \\ &+ \left(\frac{\partial \rho e}{\partial \rho}\right)_{\rho E,\rho u}\Bigg|_m^n (\rho|_m^{n+1} - \rho|_m^n) + \text{H.O.} \end{aligned}$$

$$= - F_{\rho E}\big|_m^n \Delta t + u|_m^n F_{\rho u}\big|_m^n \Delta t - \frac{1}{2}(u|_m^n)^2 F_\rho\big|_m^n \Delta t + \text{H.O.} \quad (12)$$

From Equation 12, we now substitute the split-form KEEP fluxes in Equations 2–8. We then regroup the resulting face contributions into an internal-energy advection part and two “cancellation” parts, which vanish identically under a uniform-velocity and uniform-pressure state at t_n.

$$
\begin{aligned}
\rho e|_m^{n+1} - \rho e|_m^n &= -\left[F_{\rho E}\Big|_m^n - u|_m^n \; F_{\rho u}\Big|_m^n + \frac{1}{2}\left(u|_m^n \right)^2 \; F_{\rho}\Big|_m^n \right]\Delta t + O(\Delta t^2) \\
&= -\frac{\Delta t}{\Delta x}\Bigg[\left(I|_{m+\frac{1}{2}}^n - I|_{m-\frac{1}{2}}^n \right) \\
&\quad + \left(S|_{m+\frac{1}{2}}^n - S|_{m-\frac{1}{2}}^n \right) - u|_m^n \left(\Pi|_{m+\frac{1}{2}}^n - \Pi|_{m-\frac{1}{2}}^n \right) \\
&\quad + \left(K|_{m+\frac{1}{2}}^n - K|_{m-\frac{1}{2}}^n \right) - u|_m^n \left(M|_{m+\frac{1}{2}}^n - M|_{m-\frac{1}{2}}^n \right) \\
&\quad + \frac{1}{2}\left(u|_m^n \right)^2 \left((C_1 + C_2)|_{m+\frac{1}{2}}^n - (C_1 + C_2)|_{m-\frac{1}{2}}^n \right) \Bigg] + O(\Delta t^2).
\end{aligned}
$$

Assuming a constant velocity, U_0 and pressure p_0 at t_n in Equation 3, we get

$$
\rho e|_m^{n+1} - \rho e|_m^n = -U_0 \left(\rho e|_{m+\frac{1}{2}}^n - \rho e|_{m-\frac{1}{2}}^n \right) \frac{\Delta t}{\Delta x} + O(\Delta t^2).
$$

Now, the implicit update rule for pressure can be derived for a single-step temporal scheme, employing the presumed initial condition of $u|_m^n = U_0,\; p|_m^n = p_0 \;\forall m$,

$$
\begin{aligned}
p|_m^{n+1} - p|_m^n &= \left(\frac{\partial p}{\partial \rho e}\right)_{\rho Y_1, \rho Y_2, \phi}\Bigg|_m^n \left(\rho e|_m^{n+1} - \rho e|_m^n \right) + \left(\frac{\partial p}{\partial \rho Y_1}\right)_{\rho e, \rho Y_2, \phi}\Bigg|_m^n \left(\rho Y_1|_m^{n+1} - \rho Y_1|_m^n \right) \\
&\quad + \left(\frac{\partial p}{\partial \rho Y_2}\right)_{\rho e, \rho Y_1, \phi}\Bigg|_m^n \left(\rho Y_2|_m^{n+1} - \rho Y_2|_m^n \right) + \left(\frac{\partial p}{\phi}\right)_{\rho e, \rho Y_1, \rho Y_2}\Bigg|_m^n \left(\phi|_m^{n+1} - \phi|_m^n \right) + \text{H.O.} \\
&= -\frac{U_0 \Delta t}{\Delta x} \Bigg[\left(\frac{\partial p}{\partial \rho e}\right)\Bigg|_m^n \left(\rho e|_{m+\frac{1}{2}}^n - \rho e|_{m-\frac{1}{2}}^n \right) + \left(\frac{\partial p}{\partial \rho Y_1}\right)\Bigg|_m^n \left(\rho Y_1|_{m+\frac{1}{2}}^n - \rho Y_1|_{m-\frac{1}{2}}^n \right) \\
&\quad + \left(\frac{\partial p}{\partial \rho Y_2}\right)\Bigg|_m^n \left(\rho Y_2|_{m+\frac{1}{2}}^n - \rho Y_2|_{m-\frac{1}{2}}^n \right) \Bigg] \frac{\Delta t}{\Delta x} + \left(\frac{\partial p}{\partial \phi}\right)\Bigg|_m^n \left(\phi|_{m+\frac{1}{2}}^n - \phi|_{m-\frac{1}{2}}^n \right) \Bigg] + \text{H.O.}
\end{aligned}
\tag{13}
$$

Note that the constant variables of the partial derivatives are omitted for the second equation in Eq. (13) for clarity purposes.

Similar update rules can be derived for the species temperatures, $T_1|_m^{n+1} - T_1|_m^n$ and $T_2|_m^{n+1} - T_2|_m^n$, which, when substracted from one another, results in the update rule for the species temperature balance $\Delta T \equiv T_1 - T_2$,

$$
\begin{aligned}
\Delta T|_m^{n+1} = -\frac{U_0 \Delta t}{\Delta x} \Bigg[&\left(\frac{\partial \Delta T}{\partial \rho e}\right)_{\rho Y_1, \rho Y_2, \phi}\Bigg|_m^n \left(\rho e|_{m+\frac{1}{2}}^n - \rho e|_{m-\frac{1}{2}}^n \right) \\
&+ \left(\frac{\partial \Delta T}{\partial \rho Y_1}\right)_{\rho e, \rho Y_2, \phi}\Bigg|_m^n \left(\rho Y_1|_{m+\frac{1}{2}}^n - \rho Y_1|_{m-\frac{1}{2}}^n \right) \\
&+ \left(\frac{\partial \Delta T}{\partial \rho Y_2}\right)_{\rho e, \rho Y_1, \phi}\Bigg|_m^n \left(\rho Y_2|_{m+\frac{1}{2}}^n - \rho Y_2|_{m-\frac{1}{2}}^n \right) \\
&+ \left(\frac{\partial \Delta T}{\partial \phi}\right)_{\rho e, \rho Y_1, \rho Y_2}\Bigg|_m^n \left(\phi|_{m+\frac{1}{2}}^n - \phi|_{m-\frac{1}{2}}^n \right) \Bigg] + \text{H.O.}
\end{aligned}
\tag{14}
$$

Note that the presumed initial condition of $\Delta T|_m^n = 0$ for each grid index m has also been used. This condition is always true for arbitrary solutions of the augmented five-equation system due to the thermal relaxation step.

Now, the remaining pressure and temperature balance criteria Eqs. (10) and (11) can be expressed to the leading order by equating the right-hand sides of Eqs. (13) and (14) to zero, with the short-hand

$$\epsilon_\Phi \equiv \partial(\rho e)/\partial\Phi \quad \text{and} \quad \beta_\Phi \equiv \partial\Delta T/\partial\Phi$$

for partial derivatives of the thermodynamic functions $\rho e(\rho Y_1, \rho Y_2, \phi, p)$ and $\Delta T(\rho Y_1, \rho Y_2, \rho e, \phi)$, respectively,

$$\left(\rho e|_{m+\frac{1}{2}} - \rho e|_{m-\frac{1}{2}}\right) - \epsilon_{\rho Y_1}\Big|_m \left(\rho Y1|_{m+\frac{1}{2}} - \rho Y1|_{m-\frac{1}{2}}\right) \\ - \epsilon_{\rho Y_2}\Big|_m \left(\rho Y2|_{m+\frac{1}{2}} - \rho Y2|_{m-\frac{1}{2}}\right) - \epsilon_\phi\Big|_m \left(\phi|_{m+\frac{1}{2}} - \phi|_{m-\frac{1}{2}}\right) = 0, \quad (15)$$

$$\beta_{\rho e}\Big|_m \left(\rho e|_{m+\frac{1}{2}} - \rho e|_{m-\frac{1}{2}}\right) + \beta_{\rho Y_1}\Big|_m \left(\rho Y1|_{m+\frac{1}{2}} - \rho Y1|_{m-\frac{1}{2}}\right) \\ + \beta_{\rho Y_2}\Big|_m \left(\rho Y2|_{m+\frac{1}{2}} - \rho Y2|_{m-\frac{1}{2}}\right) + \beta_\phi\Big|_m \left(\phi|_{m+\frac{1}{2}} - \phi|_{m-\frac{1}{2}}\right) = 0. \quad (16)$$

We emphasize that the pressure-equilibrium criteria derived above is only *spatially* exact, in the sense that pressure error converges with the same (linear) rate with time step size for all mesh spacings. This is a common property of pressure-equilibrium preserving conservative methods [6, 8] since we only explicitly update the conservative variables $(\rho Y_k, \rho u, \rho E)$, along with the augmented volume fraction ϕ. Nonetheless, relative to the traditional KEEP discretization, the present approach removes the need to rely on mesh refinement to recover pressure equilibrium, since the spatial PEP condition is enforced independently of Δx. Any remaining pressure error in the fully discrete scheme is then attributable to the time discretization and is proportional to the time-step size, i.e., $O(\Delta t)$ for the single-step update used in this derivation. Higher-order temporal variants can be constructed by applying standard multi-stage or multi-step integrators to the same Euler-type updates presented here, which would yield $O(\Delta t^q)$ temporal error for a qth-order method. Extensions of the above analysis to higher-order truncations in Δt will be the subject of future work.

The question of interest is then the choice of mid-point values

$$\mathbf{f}|_{m+\frac{1}{2}} \equiv \left[\rho Y1|_{m+\frac{1}{2}} \;\; \rho Y2|_{m+\frac{1}{2}} \;\; \phi|_{m+\frac{1}{2}} \;\; \rho e|_{m+\frac{1}{2}}\right]^T$$

to satisfy the dual constraints Eqs. (15) and (16).

Extending our previous work [8] to the augmented five-equation model, the solution to the criteria Eqs. (15) and (16) can be obtained via splitting up the criteria and shifting the second parts by one cell, resulting in a linear constraint on the mid-point values,

$$\mathbf{A}|_{m+\frac{1}{2}}\, \mathbf{c}|_{m+\frac{1}{2}} = \mathbf{b}|_{m+\frac{1}{2}} - \mathbf{A}|_{m+\frac{1}{2}}\, \mathbf{f^0}\Big|_{m+\frac{1}{2}}, \quad (17)$$

where

$$\mathbf{f}|_{m+\frac{1}{2}} = \mathbf{f^0}\Big|_{m+\frac{1}{2}} + \mathbf{c}|_{m+\frac{1}{2}}. \quad (18)$$

Here, the mid-point values are decomposed into a generic base-line scheme, $\mathbf{f^0}$, and a correction $\mathbf{c}$. This decomposition is specifically made to improve floating-point robustness of the algorithm under the removable singularity when the flow states at cells m and $m+1$ are identical. In this paper, we choose to use algebraic-mean for the base-line mid-point values $\mathbf{f^0}$, as commonly used in the standard KEEP scheme [10]. Furthermore, the forms of $\mathbf{A}$ and $\mathbf{b}$ are

$$\mathbf{A}|_{m+\frac{1}{2}} = \begin{pmatrix} -\epsilon_{\rho Y_1}\big|_m & -\epsilon_{\rho Y_2}\big|_m & -\epsilon_{\phi}\big|_m & 1 \\ -\epsilon_{\rho Y_1}\big|_{m+1} & -\epsilon_{\rho Y_2}\big|_{m+1} & -\epsilon_{\phi}\big|_{m+1} & 1 \\ \beta_{\rho Y_1}\big|_m & \beta_{\rho Y_2}\big|_m & \beta_{\phi}\big|_m & \beta_{\rho e}\big|_m \\ \beta_{\rho Y_1}\big|_{m+1} & \beta_{\rho Y_2}\big|_{m+1} & \beta_{\phi}\big|_{m+1} & \beta_{\rho e}\big|_{m+1} \end{pmatrix},$$
$$\mathbf{b}|_{m+\frac{1}{2}} = \begin{pmatrix} \rho e|_m - \epsilon_{\rho Y_1}\big|_m \rho Y_1|_m - \epsilon_{\rho Y_2}\big|_m \rho Y_2|_m - \epsilon_{\phi}\big|_m \phi|_m \\ \rho e|_{m+1} - \epsilon_{\rho Y_1}\big|_{m+1} \rho Y_1|_{m+1} - \epsilon_{\rho Y_2}\big|_{m+1} \rho Y_2|_{m+1} - \epsilon_{\phi}\big|_{m+1} \phi|_{m+1} \\ \beta_{\rho e}\big|_m \rho e|_m + \beta_{\rho Y_1}\big|_m \rho Y_1|_m + \beta_{\rho Y_2}\big|_m \rho Y_2|_m + \beta_{\phi}\big|_m \phi|_m \\ \beta_{\rho e}\big|_{m+1} \rho e|_{m+1} + \beta_{\rho Y_1}\big|_{m+1} \rho Y_1|_{m+1} + \beta_{\rho Y_2}\big|_{m+1} \rho Y_2|_{m+1} + \beta_{\phi}\big|_{m+1} \phi|_{m+1} \end{pmatrix}, \tag{19}$$

Here, we emphasize two key points: (a) the construction of the mid-point corrections is general and can be applied to any consistent choice of baseline mid-point values, and (b) the proposed correction ensures exact pressure-equilibrium preservation at any mesh resolution, subject only to temporal errors introduced by the time-stepping method.

As highlighted in [8], direct solution of Eq. (19) is not ideal due to the limiting behavior of the PEP construction at infinite resolution, i.e., when the flow states to the left and right of the mid-point approach one another, $q|_{m+1} \rightarrow q|_m$. At this point, the linear problem Eq. (19) has no defined solution since $\mathbf{A}|_{m+\frac{1}{2}}$ becomes singular and $\mathbf{b}|_{m+\frac{1}{2}} \rightarrow \mathbf{0}$. Nonetheless, analysis of the PEP construction for the four-equation system in [8] shows that the approach to singularity in the left-hand-side matrix $\mathbf{A}$ is linear with respect to the difference in the flow state between cell m and $(m+1)$, while the approach to singularity in the right-hand-side vector $\mathbf{b}$ is quadratic. We expect the same property to hold for the present extension to the five-equation system. Thus,

$$\lim_{\mathbf{q}|_{m+1} \rightarrow \mathbf{q}|_m} \mathbf{c}|_{m+\frac{1}{2}} = \mathbf{0}. \tag{20}$$

Then, since the underlying KEEP scheme is a consistent flux, the combination with the PEP correction term is also consistent. Nonetheless, careful treatment of the removable singularity in the linear system Eq. (19) is required for robust numerical evaluation of the PEP correction. Specifically, the Moore–Penrose pseudoinverse is employed to obtain the solution to the linear system, since its output correctly relaxes to $\mathbf{0}$ when the left-hand side matrix is singular. The tolerance of the pseudoinverse algorithm, which controls the threshold for discarding eigenvalues in the decomposition of $\mathbf{A}|_{m+\frac{1}{2}}$ is set to 10^{-12} for this work.

4. Test results of the proposed PEP scheme

4.1 One-dimensional advection

We consider a free-stream preservation simulation of a water/air mixture with sinusoidal initial profiles of composition and temperature,

$$\begin{aligned} p(0,x) &= 101325 \text{ (Pa)} \\ u(0,x) &= 100 \text{ (m/s)} \\ \phi(0,x) &= 0.8(0.5 - 0.5\sin(4\pi x)) + 0.1 \\ T(0,x) &= 200(0.5 - 0.5\sin(4\pi x)) + 300 \text{ (K)}. \end{aligned}$$

Note that the choice of a varying initial temperature profile is deliberate to excite the pressure/velocity disequilibrium mode of the five-equation system. Furthermore the the stiffened-gas properties of the water/air mixture is summarized in Table 1.

The simulation is performed on a 1D periodic domain in $x \in [0, 1]$ m with the 3-stage, 3rd-order explicit optimal Strong Stability-Preserving Runge-Kutta (SSPRK33) time stepping scheme on a 128-cell grid

Table 1: Stiffened-gas properties for water and air.

	Water	Air
p_∞	1e9	0
q	-1.167e6	0
c_v	1816	719.3
γ	2.35	1.4

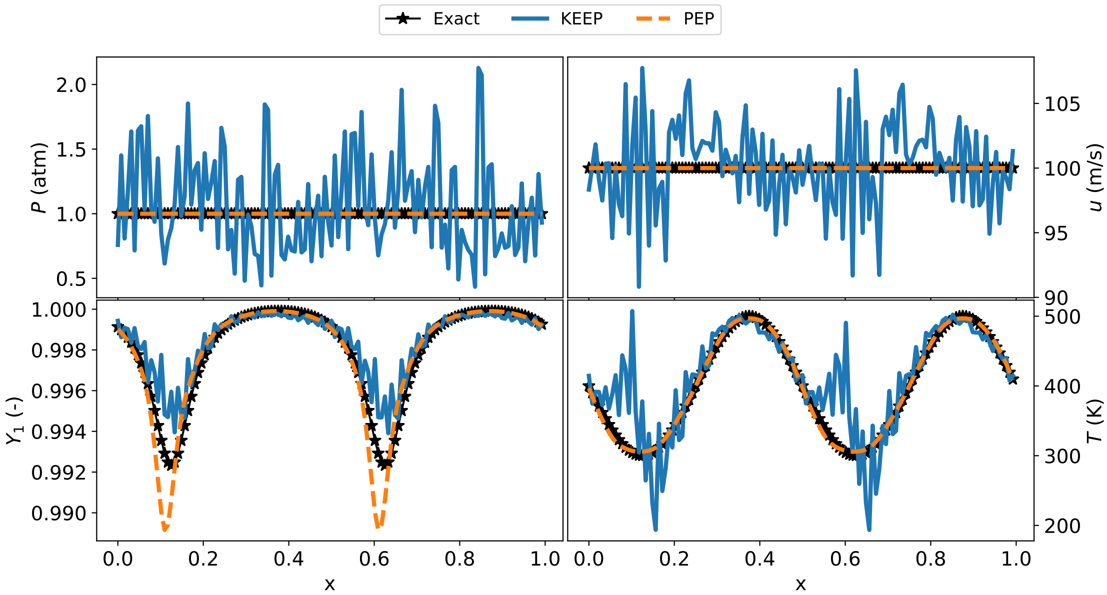

Figure 1: Solution of the 1D sinusoidal advection test comparing the proposed PEP scheme (red), the standard KEEP scheme (blue), and the exact solution (black) after three FTTs. The final velocity and pressure profiles obtained with the proposed PEP scheme match the exact solution to the pseudoinverse tolerance.

with CFL = 0.8.

Figure 1 compare the simulation results after three flow-through times (FTTs) using the standard split KEEP scheme and the proposed PEP correction. It can be observed that proposed PEP scheme successfully eliminates the pressure/velocity disequilibrium observed in the standard KEEP scheme.

Results of the convergence study of the proposed PEP scheme is shown in Fig. 2. We find that the correct second-order convergence is observed for the advected flow variables, in this case liquid-phase mass-fraction, see Fig. 2a. This is the convergence property of the underlying KEEP scheme. On the hand, since the pressure-equilibrium preservation of the proposed PEP scheme is *spatially* exact, we find in Fig. 2b that the pressure error now converges with the order of the time integrator (in this case $O(\Delta t^3)$, which is translated to $O(\Delta x^3)$ via the CFL = 0.8 condition). The relative pressure error then plateaus at 10^{-9} due to the tolerance used in the pseudo-inverse solution of Eq. (17).

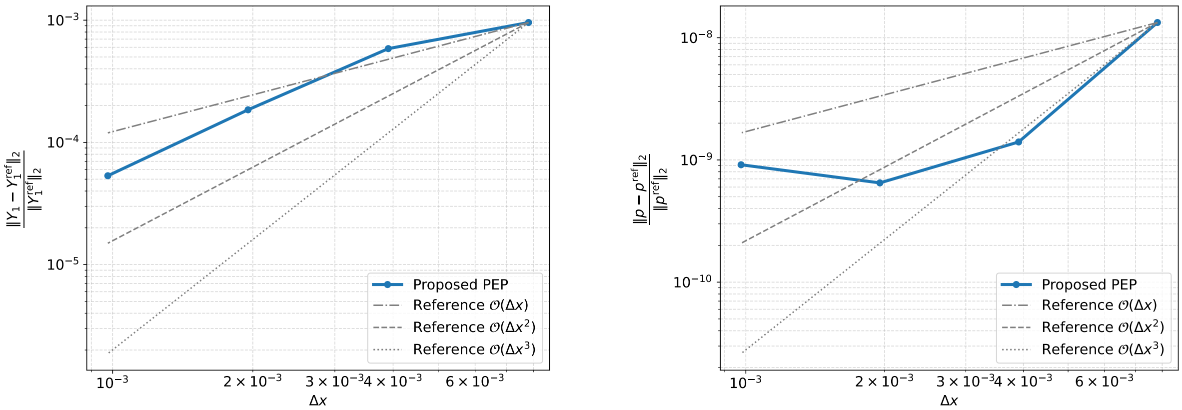

(a) Liquid-phase mass fraction convergence

(b) Pressure convergence

Figure 2: Convergence study for liquid-phase mass-fraction and pressure for the one-dimensional advection configuration with the PEP scheme after three FTTs.

4.2 Two-dimensional advection

The free-stream preservation test case is further extend to two dimensions by considering a diagonally advected water-air mixture with the following initial condition

$$
\begin{aligned}
p(0,x) &= 101325 \text{ (Pa)}\\
u(0,x) &= 100 \text{ (m/s)}\\
v(0,x) &= 100 \text{ (m/s)}\\
\phi(0,x) &= 0.8(0.5-0.5\sin(4\pi x))(0.5-0.5\sin(4\pi y))+0.1\\
T(0,x) &= 200(0.5-0.5\sin(4\pi x))(0.5-0.5\sin(4\pi y))+300 \text{ (K)}.
\end{aligned}
\tag{21}
$$

The simulation is performed on a 2D periodic domain in $(x, y) \in [(0,0),(1,1)]$ m with SSPRK3 time stepping scheme on a 128×128-cell grid with CFL $= 0.8$. Figure 3 shows the profiles of pressure and velocity after three FTTs. The proposed PEP scheme is able to maintain the equilibrium of pressure and velocity exactly, while the standard split KEEP scheme produces large-amplitude oscillations. These instabilities in the KEEP scheme result in poor solution of the flow's density and temperature fields at this final time, as shown in Fig. 4a. In contrast, the final profiles of density and temperature are well preserved when advected using the proposed PEP scheme, see Fig. 4b.

5. Experimental construction of a hybrid upwind/central-PEP scheme

We have demonstrated that the proposed modification of the KEEP scheme dramatically improves its ability to preserve pressure equilibrium. However, the PEP modification is not appropriate in flow regions where pressure and velocity are not in equilibrium. Similarly, KEEP schemes are non-dissipative and, despite their enhanced numerical stability, are only suited for smooth flow regions. Compressible flows of engineering interest often have strong solution discontinuities.

To address these deficiencies of the proposed central-PEP construction, further treatments are needed. One promising approach is via hybridization of the flux by blending the central KEEP-PEP flux with a stable upwind flux such as approximate Riemann solvers. This development is currently under active research. In this section, we present a proof-of-concept of the idea by considering the dynamics of the hybrid blending of the proposed central PEP scheme with the HLLEC flux [11] with first-order mid-point

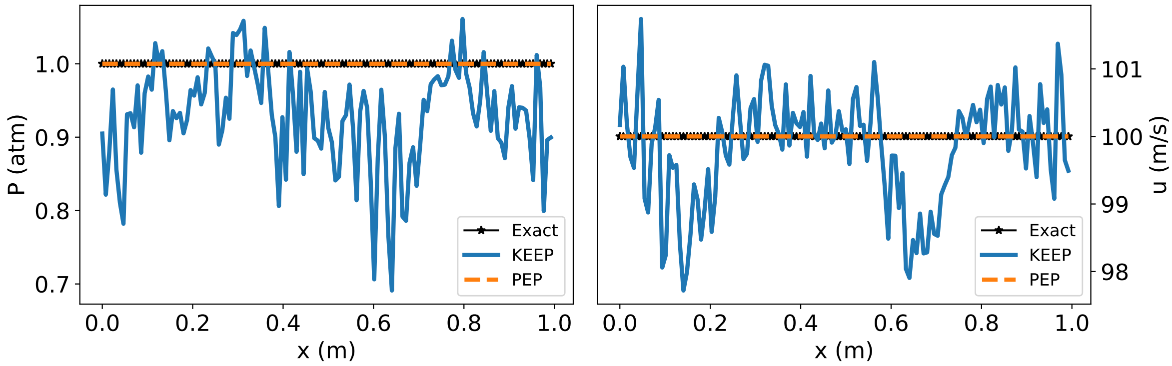

Figure 3: Solution profiles of pressure and velocity at $y = 0.5$ m for the two-dimensional advection problem. Comparison is make between the proposed PEP scheme (red), the standard KEEP scheme (blue), and the exact solution (black) after three FTTs. The final velocity and pressure profiles obtained with the proposed PEP scheme match the exact solution to the pseudoinverse tolerance.

interpolation,

$$\mathbf{f}|_{m+\frac{1}{2}} = (1 - \zeta|_{m+\frac{1}{2}})(\mathbf{f}_{\text{KEEP}}|_{m+\frac{1}{2}} + \alpha\, \mathbf{c}|_{m+\frac{1}{2}}) + \zeta|_{m+\frac{1}{2}}\, \mathbf{f}_{\text{HLLEC}}|_{m+\frac{1}{2}}\,, \tag{22}$$

where ζ is a shock sensor used to detect regions of flow discontinuity and numerical stability problems where the dissipative HLLEC flux can be injected. Here, we use for ζ a combination of the WENO sensor [12] and a wiggle sensor for pressure and density.

In Eq. (22), we also employ a second sensor α to detect regions of near equilibria in pressure and velocity, such that the PEP correction to the KEEP scheme, see Eq. (18), can be activated. The form of the sensor α is

$$\alpha|_{m+\frac{1}{2}} \equiv \sin\left(\frac{\pi}{2} \cdot \min\left(1 - \min\left(\frac{a|_{m+\frac{1}{2}} - a_{\text{lb}}}{a_{\text{ub}} - a_{\text{lb}}}, 1\right), 1\right)\right), \tag{23}$$

where a is a measure of the jump in pressure and velocity between the two adjacent cells

$$a|_{m+\frac{1}{2}} \equiv \max\left(\frac{\left|p|_{m+1} - p|_m\right|}{\max\left(p|_{m+1}\,,\, p|_m\right)}, \frac{\left|u|_{m+1} - u|_m\right|}{\max\left(s|_{m+1}\,,\, s|_m\right)}\right), \tag{24}$$

and $a_{\text{lb}}, a_{\text{ub}}$ are user-controlled parameter to define the start and end points of the ramping of the PEP correction. Lastly, note that s is the fluid's sound speed.

5.1 One-dimensional advection

We first demonstrate the stability of the hybrid flux scheme Eq. (22) on the one-dimensional advection configuration studied in Section 4.1.

To evaluate the central/upwind flux blending, Figure 5 compares the solution profiles of pressure and velocity after three FTTs for five values of the blending factor ζ. Note that the PEP correction blending α is fixed to unity for this test. Furthermore, that the grid resolution is increased to 256 cells to maintain stability of the PEP correction when deployed to pressure/velocity disequilibrium flow fields generated by the upwind flux.

When $\zeta = 0$, the central PEP scheme is exactly recovered and pressure equilibrium is preserved exactly. With increasing ζ, the influence of the HLLEC flux leads to increasing fluctuations in the pressure and velocity profiles. Nonetheless, it can be observed that the correction terms of the central PEP scheme remains stable under these pressure/velocity oscillations induced by the upwind flux. Overall, this test

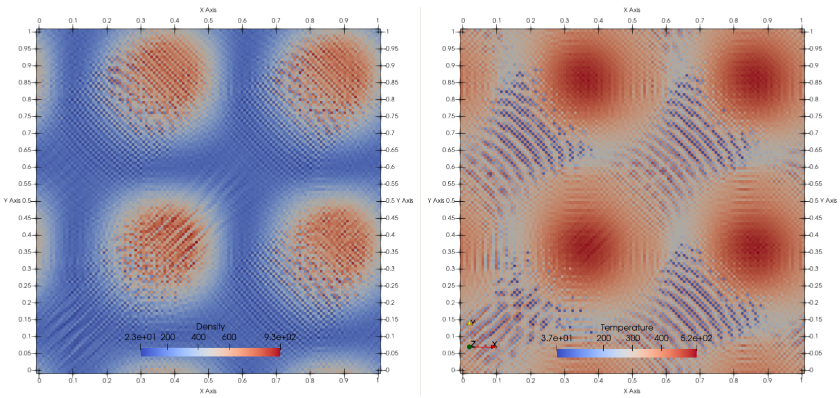

(a) KEEP

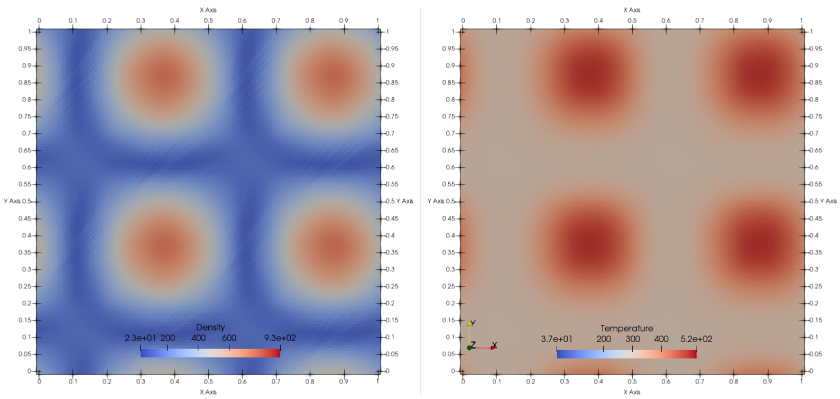

(b) PEP

Figure 4: Solution of the 2D sinusoidal advection test comparing the profiles of density (left) and temperature (right) obtained from the standard split KEEP scheme and the proposed PEP scheme after three FTTs.

also demonstrates the ability to surgically blend in the central PEP scheme with a dissipative upwind flux to control pressure equilibrium error.

We emphasize that the hybrid central/upwind flux scheme alone is still unable to fully suppress numerical instability at the shock due to the application of the PEP correction at this region of pressure discontinuity. Alleviating this requires the addition of the second blending factor to only activate the PEP correction **c** in pressure-equilibrium regions. To evaluate the ability of the PEP-correction blending sensor α on stabilizing the application of PEP into flow fields with pressure/velocity disequilibrium, we perform the one-dimensional advection test case again, but with a dynamic shock sensor ζ to blend in the HLLEC upwind flux, introducing dissipation and thus pressure variations into the flow. To promote the activation of the WENO shock sensors near the extrema of the sinusoidal profiles in mass fraction and temperature, we use a coarser mesh size of 128 cells for this test.

Figure 6 presents simulation results for three configurations of the PEP blending sensor α. We observe that the more liberal blending of the PEP correction (in the case of $a_{\text{ub}} = 10^{-4}$), the addition of the PEP correction terms actually destabilizes the flow since it is being employed in regions of pressure/velocity disequilibrium, induced by the application of the dissipative upwind flux. One approach to alleviate this issue is the construction and application of a second PEP correction to the HLLEC flux, which is the subject of ongoing work. We also found that more limited application of the PEP correction to regions of near pressure equilibrium (in the case of $a_{\text{ub}} = 10^{-5}$) provides some marginal improvement in flow stability compared to the no PEP approach. However, the improvement is very limited in this case, but we expect to obtain better results of the PEP correction when it is also applied to the HLLEC upwind flux scheme.

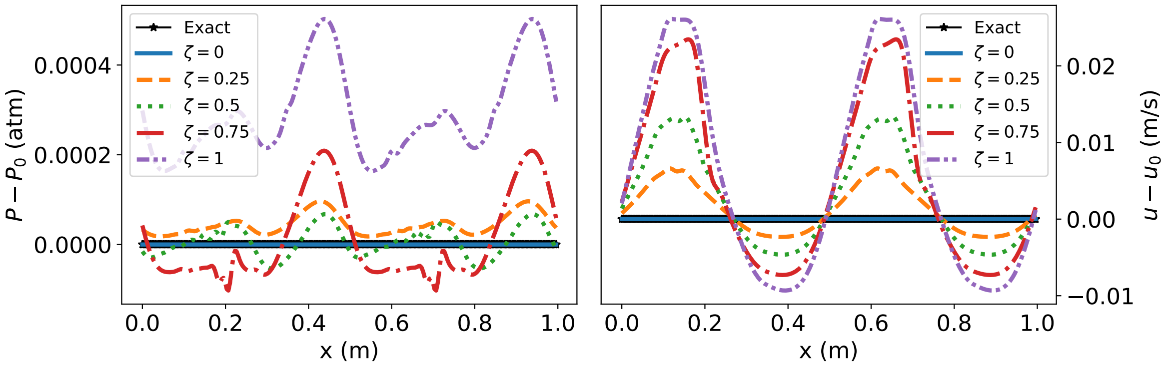

Figure 5: Solution profiles of pressure and velocity at three FTTs for the one-dimensional advection problem with 256 cells using the hybrid flux scheme. Comparison is made between five values of the central/upwind blending factor ζ. The PEP correction is always fully applied with $\alpha = 1$.

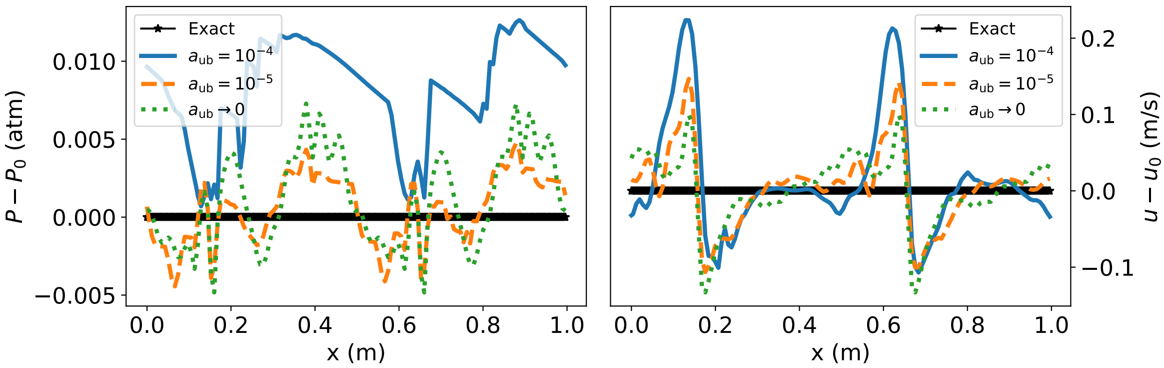

Figure 6: Solution profiles with of pressure and velocity at three FTTs for the one-dimensional advection problem with 128 cells using the hybrid flux scheme and dynamic PEP-correction activation. Comparison is made between three configurations of the equilibrium sensor α: $a_{\mathrm{ub}} = 10^{-4}$, $a_{\mathrm{ub}} = 10^{-5}$, and $a_{\mathrm{ub}} \to 0$ (limit of no PEP correction). Note that $a_{\mathrm{lb}} = a_{\mathrm{ub}}/2$ for this test. The WENO/wiggle shock sensor for the hybrid central/upwind blending factor ζ is employed here.

5.2 Two-phase shock configurations

To further demonstrate the ability of the hybrid-flux and dynamic-PEP-correction approach to bridge the gap between the central PEP scheme and general flow configuration with discontinuities, we deploy the flux scheme in Eq. (22) on two canonical two-phase shock configuration.

5.2.1 One-dimensional Sod shock tube

First, we consider a one-dimensional two-phase Sod shock tube configuration with water and air with the initial conditions

$$[p, u, Y_{\mathrm{liq}}, T] = \begin{cases} [10^9 \text{ Pa}, 0, 1, 300 \text{ K}] \text{ if } x < 0.8 \text{ m} \\ [10^5 \text{ Pa}, 0, 0, 300 \text{ K}] \text{ if } x > 0.8 \text{ m} \end{cases}. \tag{25}$$

The configuration is solved on the domain $x \in [0, 1.6]$ m with a 400-cell grid. The configuration for the PEP-correction activation sensor is $a_{\mathrm{ub}} = 0.4$ and $a_{\mathrm{lb}} = 0.1$. We found that for shock configurations, the variations in pressure and velocities are higher in the domain, necessitating the increase in the threshold of pressure/velocity differences below which the PEP correction is activated. Nonetheless, it was observed

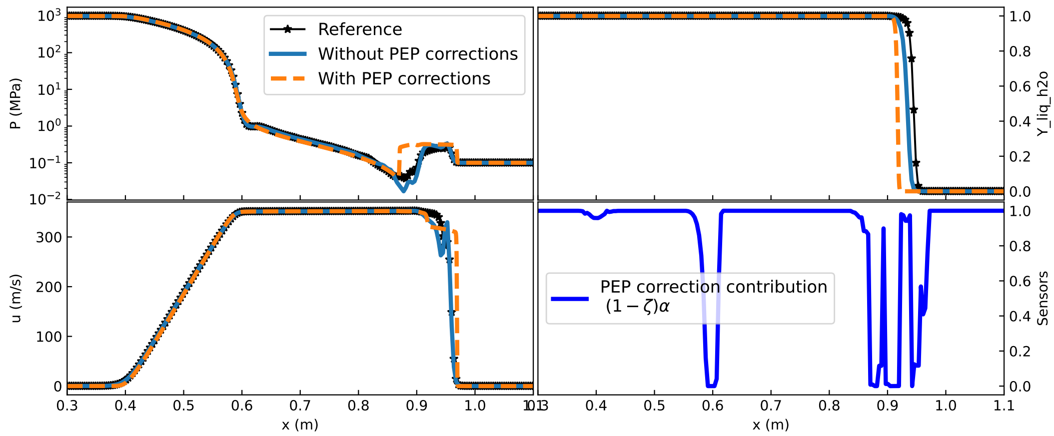

Figure 7: Hybrid-flux solution profiles of pressure, liquid mass fraction, and velocity for the one-dimensional two-phase Sod problem at $t = 30$ ms. Copmparison is made between simulations with and without the dynamic activation of PEP correction and a reference solution. Also shown is the dynamic contribution of the PEP correction term $(1 - \zeta)\alpha$.

that the stabilization effect of the PEP correction is apparent in this configuration, despite the more liberal use of the correction term in regions of pressure/velocity disequilibrium.

The solution at time $t = 30$ ms is shown in Fig. 7. We observe that the hybrid-flux formulation remains stable for this simulation involving discontinuities and regions of pressure/velocity disequilibrium. The shock sensor is only activated to avoid oscillations around the shock and contact line, while the central PEP scheme is the monolithic flux for the rest of the domain, including across the rarefaction fan. Furthermore, we also observe that the PEP-correction activation sensor is active for most of the domain, except for across the shock and at the top of the rarefaction fan. Compared with the simulation without PEP corrections, the ability of the central PEP scheme to stabilize the solution across the liquid/air contact line is apparent, where the overshoots in pressure and velocity are greatly reduced. Nonetheless, we observe that the comparison with the reference solution, obtained with a first-order HLLEC simulation with 20000 cells, remains limited, especially in the region between the rarefaction fan and the shock.

5.2.2 Two-dimensional shock/water-column interaction

The stability of the hybrid flux Eq. (22) is further tested in a two-dimensional shock/water-cylinder interaction configuration. In this problem, a Mach 1.47 shock wave in air interacts with a water column with initial diameter $D = 4.8$ mm. The pre-shock air and liquid water are initially at atmospheric conditions with $p = 101325$ Pa and $T = 298$ K. The resolution of the simulation is 50 cells per droplet diameter.

Solution of the shock/water-cylinder interaction is present in Fig. 8 for a snapshot at $t = 146$ μs, showing a comparison between the hybrid flux Eq. (22) with and without the dynamic PEP corrections.

We find that the hybrid flux scheme with dynamic PEP corrections remains robust for this configuration, where the PEP scheme performs well in maintaining pressure equilibrium across the liquid/vapor contact line. This is evident by the smoother leading edge of the droplet compared to the simulation result without PEP corrections. However, spurious grid-to-grid oscillations are observed in the wake of the water column, where the PEP scheme is introducing numerical artifacts due to it being unsuitable in regions of pressure/velocity disequilibrium.

It is emphasized that for this shock/water-cylinder configuration, the configuration of the PEP-activation

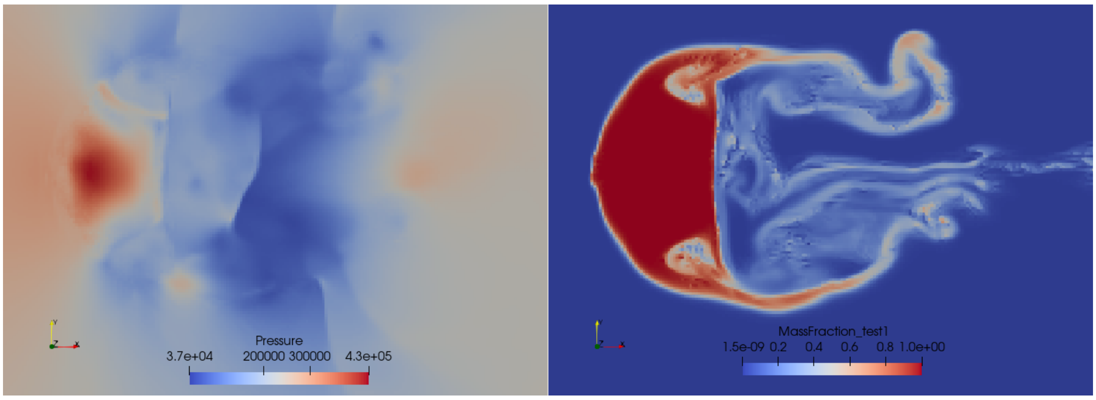

(a) With PEP corrections

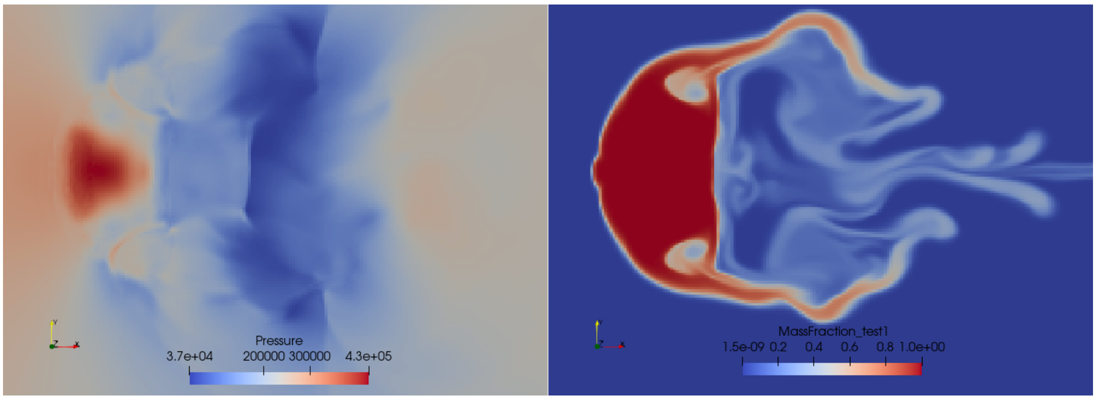

(b) Without PEP corrections

Figure 8: Solution of the two-dimensional shock/water-column interaction configuration using the hybrid scheme. Pressure and liquid mass fraction are shown a snapshot at $t = 146$ μs. Comparison is made between simulation obtained (a) with PEP corrections and (b) without PEP corrections to the central KEEP flux scheme. Improvement in resolution of the contact line is observed from the leading edge of the droplet in panel (a). However, incorrect activation of the PEP corrections in the wake region results in numerical artifacts.

sensor is $a_{\text{ub}} = 0.01$ and $a_{\text{lb}} = 0.005$, which is decreased from the Sod shock tube configuration to limit the activation of the PEP correction terms in the wake of the column. As such, we highlight that the current blending and PEP activation strategy is still problematic due to the wide range of the tunable parameters a_{ub} and a_{lb} to maintain a balance between sufficient activation of the PEP correction and avoiding applying the PEP corrections in regions of pressure/velocity disequilibrium where they are not applicable. The inappropriate application of the PEP correction terms into the wake is the cause of the flow instability observed in Fig. 8a. We hypothesize that this is due to the incorrect use of the speed-of-sound as the scaling for velocity disequilibrium in Eq. (24). Applying a sensor that more directly measures pressure disquilibrium, such as a point-wise approximation of the local $\partial P/\partial t$, may overcome these robustness issues.

6. Conclusions

In this work, we present the construction of an *spatially-exact*, fully-conservative, central PEP scheme for Allaire's five-equation model coupled with thermal relaxation. Combined with a suitable upwind flux for regions of strong pressure gradients, the proposed scheme promises enhanced robustness compared to traditional four-equation methods. In particular, the central PEP scheme improves the numerical stability of contact-line advection, while the hyperbolic step of the augmented system, with its monotonic sound-speed variation, ensures stable and accurate shock propagation across material interfaces [5].

The construction of the central PEP scheme *guarantees* pressure equilibrium of the augmented five-equation system at flow regions where pressure and velocity are near constant. This was demonstrated for one-dimensional and two-dimensional advection tests, showing pressure error at the pseudoinverse tolerance at moderate grid resolutions. At the limit of coarse meshes, pressure error was found to converge with the order of the time-stepping scheme. The construction of the PEP correction terms assumes a first-order Euler time-integration scheme and derived the pressure-equilibrium criterion to converge with first order in time. The automatic extension of the truncation errors in the pressure-equilibrium criterion to multi-stage time-integration scheme is suggested from the convergence result with RK4 time integration, but more analysis is needed to conclusively show this.

One outstanding issue with the proposed central PEP scheme is that it is not necessarily applicable to regions of strong pressure/velocity disequilibrium, such as at shock discontinuities. While the central PEP flux is consistent, it does not carry the dissipation needed to capture shocks. Furthermore, the construction of the correction terms in the central PEP flux does not provide any guarantee of pressure stability when the initial pressure and velocity fields are not already constant. Overcoming this challenge is an ongoing research task, where our central approach is to employ a hybrid flux scheme that (a) blends the central scheme with a dissipative upwind flux and (b) only employs the PEP correction terms in regions of near-equilibrium pressure. We showed a proof-of-concept for this approach with a hybrid blending between the proposed central PEP scheme with a shock-capturing HLLEC Riemann solver. While robustness is observed for a range of one-dimensional and two-dimensional problems, the hybrid flux method still exhibits some numerical instabilities when the blending sensor fails to disable the PEP flux scheme in regions of strong pressure or velocity variations.

Acknowledgements

This work was funded by the Exploration Ground Systems (EGS) Project and Transformational Tools and Technologies (TTT) Project at NASA. Computational resources was provided by NASA's High-End Computing (HEC) Program and the NASA Advanced Supercomputing (NAS) Division at Ames Research Center.

References

[1] Melvin R Baer and Jace W Nunziato. A two-phase mixture theory for the deflagration-to-detonation transition (ddt) in reactive granular materials. *International journal of multiphase flow*, 12(6): 861–889, 1986.

[2] Grégoire Allaire, Sébastien Clerc, and Samuel Kokh. A five-equation model for the simulation of interfaces between compressible fluids. *Journal of Computational Physics*, 181(2):577–616, 2002.

[3] Tore Flåtten and Halvor Lund. Relaxation two-phase flow models and the subcharacteristic condition. *Mathematical Models and Methods in Applied Sciences*, 21(12):2379–2407, 2011.

[4] S Le Martelot, Richard Saurel, and Boniface Nkonga. Towards the direct numerical simulation of nucleate boiling flows. *International Journal of Multiphase Flow*, 66:62–78, 2014.

[5] Man Long Wong, Jordan B Angel, and Cetin C Kiris. A positivity-preserving Eulerian two-phase approach with thermal relaxation for compressible flows with a liquid and gases. *arXiv preprint arXiv:2208.04488*, 2022.

[6] Yuji Fujiwara, Yoshiharu Tamaki, and Soshi Kawai. Fully conservative and pressure-equilibrium preserving scheme for compressible multi-component flows. *Journal of Computational Physics*, 478:111973, 2023.

[7] Hiroshi Terashima, Nguyen Ly, and Matthias Ihme. Approximately pressure-equilibrium-preserving scheme for fully conservative simulations of compressible multi-species and real-fluid interfacial flows. *Journal of Computational Physics*, 524:113701, 2025.

[8] Christopher DeGrendele, Nguyen Ly, Francois Cadieux, Michael Barad, Dongwook Lee, and Jared

Duensing. On the construction of high-order and exact pressure equilibrium schemes for arbitrary equations of state. *arXiv preprint arXiv:2512.04450*, 2025.

[9] Johan Larsson and Bertil Gustafsson. Stability criteria for hybrid difference methods. *Journal of Computational Physics*, 227(5):2886–2898, 2008.

[10] Yuichi Kuya, Kosuke Totani, and Soshi Kawai. Kinetic energy and entropy preserving schemes for compressible flows by split convective forms. *Journal of Computational Physics*, 375, 2018.

[11] Eleuterio F Toro. *Riemann solvers and numerical methods for fluid dynamics: a practical introduction*. Springer Science & Business Media, 2013.

[12] Guang-Shan Jiang and Chi-Wang Shu. Efficient implementation of weighted eno schemes. *Journal of computational physics*, 126(1):202–228, 1996.